# Supplementary Information

# Ligand recognition mechanism of the human relaxin family peptide receptor 4 (RXFP4)

Brief description of what this file includes:

Supplementary Table 4 | Cell surface expression and effects of residues mutation on ligands-mediated inhibition of forskolin-induced cAMP accumulation.

Supplementary Table 5 | Effects of key residue mutation on receptor subtype selectivity.

Supplementary Table 6 | Primers used in this study, related to Figures 2 and 3, Supplementary Figures 3 and 10 and Supplementary Tables 3, 4 and 5.

Supplementary Table 7 | Details of restraints applied during MD simulations.

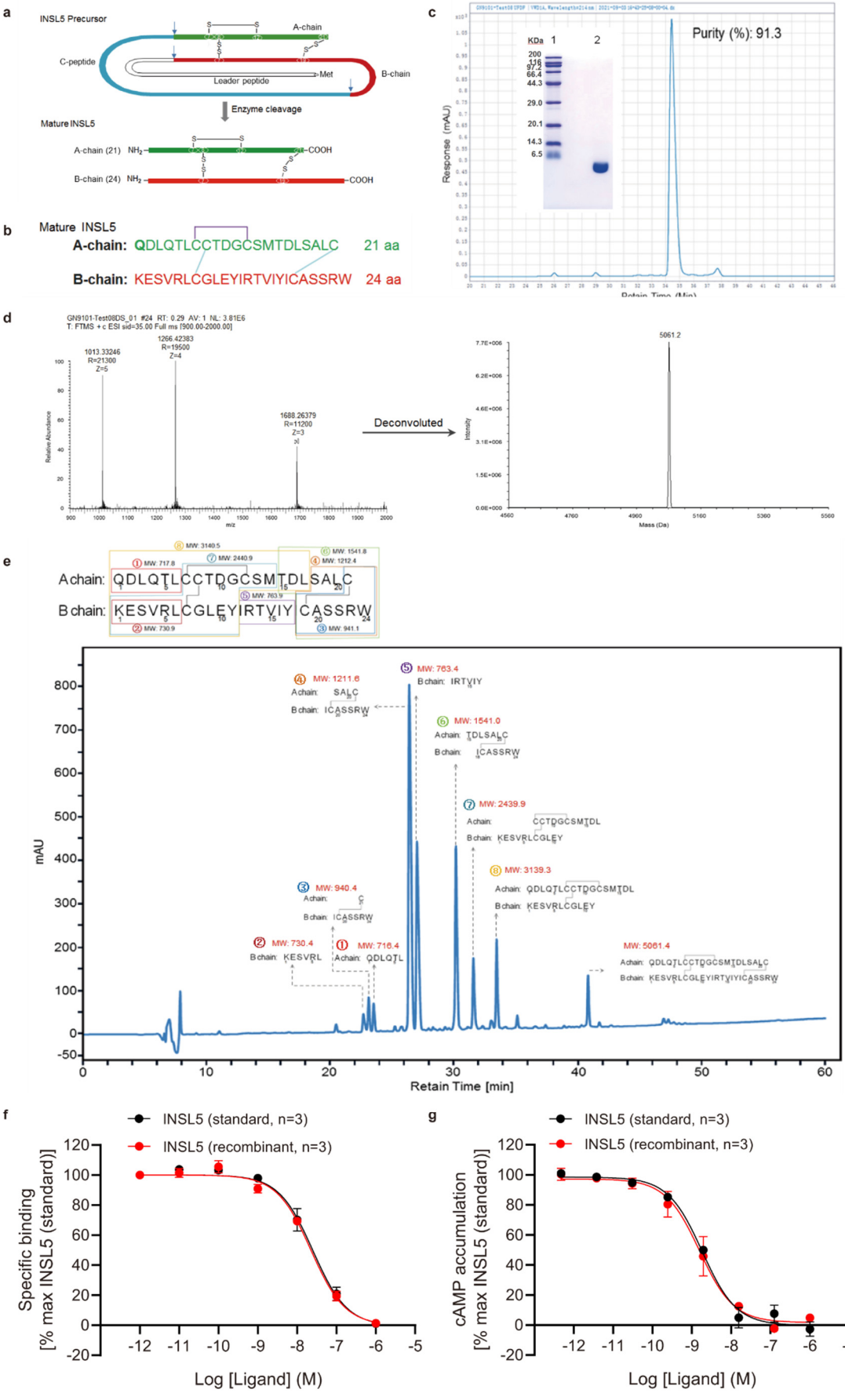
a
INSL5 Precursor
A-chain
C-peptide
Leader peptide
Met
B-chain
Enzyme cleavage
Mature INSL5
A-chain (21) NH2 COOH
B-chain (24) NH2 COOH
b
Mature INSL5
A-chain: QDLQTLCCTDGCSMTDLSALC 21 aa
B-chain: KESVRLCGLEYIRTVIYICASSRW 24 aa
c
KDa 1 2
200
116
97.2
66.4
44.3
29.0
20.1
14.3
6.5
Purity (%): 91.3
Response (mAU)
d
1013.33246 R=21300 Z=5
1266.42383 R=19500 Z=4
1688.26379 R=11200 Z=3
Deconvoluted
5061.2
Intensity
Mass (Da)
e
A chain: QDLQTLCCTDGCSMTDLSALC
B chain: KESVRLCGLEYIRTVIY CASSRW
MW: 3140.5
MW: 717.8
MW: 2440.9
MW: 1541.8
MW: 1212.4
MW: 763.9
MW: 730.9
MW: 941.1
MW: 1211.6
A chain: SALC
B chain: ICASSRW
MW: 763.4
B chain: IRTVIY
MW: 1541.0
A chain: TDLSALC
B chain: ICASSRW
MW: 2439.9
A chain: CCTDGCSMTDL
B chain: KESVRLCGLEY
MW: 3139.3
A chain: QDLQTLCCTDGCSMTDL
B chain: KESVRLCGLEY
MW: 940.4
A chain: C
B chain: ICASSRW
MW: 730.4
B chain: KESVRL
MW: 716.4
A chain: QDLQTL
MW: 5061.4
A chain: QDLQTLCCTDGCSMTDLSALC
B chain: KESVRLCGLEYIRTVIYICASSRW
mAU
Retain Time [min]
f
INSL5 (standard, n=3)
INSL5 (recombinant, n=3)
Specific binding [% max INSL5 (standard)]
Log [Ligand] (M)
g
INSL5 (standard, n=3)
INSL5 (recombinant, n=3)
cAMP accumulation [% max INSL5 (standard)]
Log [Ligand] (M)

**Supplementary Figure 1. Characterization of recombinant INSL5. a,** The structure of the INSL5 precursor and its conversion to mature INSL5. **b,** Amino acid sequence of the recombinant INSL5 used in this study. The dash indicates disulfide bond. **c,** Purity analysis of recombinant INSL5 by non-reducing SDS-PAGE and (reverse phase high-performance liquid chromatography) RP-HPLC. Well 1 is the marker, well 2 is a typical batch of recombinant INSL5. These experiments were repeated independently three times with similar results. The purity of INSL5 in this batch is 91.3%. **d,** Mass spectrometry (MS) analysis of INSL5. The measured molecular mass of 5,061.2 Da corresponds to the expected value (5,062.9 Da) of the INSL5 (N-terminal Q of A chain not converted to pE). **e,** Chymotrypsin-generated peptide mapping by liquid chromatograph (LC)-LC/MS and assignments for the amino acid sequences of the peptides. Measured molecular mass in red; structure assignment and theoretical molecular weights in black. **f-g,** The recombinant INSL5 was able to bind and activate RXFP4 as determined by europium-labeled ligand competitive binding **(f)** and cAMP accumulation assays **(g)** compared to INSL5 (standard), a control peptide containing native amino acids (N-terminal Q of A chain converted to pE). Data shown are means ± S.E.M. of three independent experiments labeled in the parentheses. Source data are provided as a Source Data file.

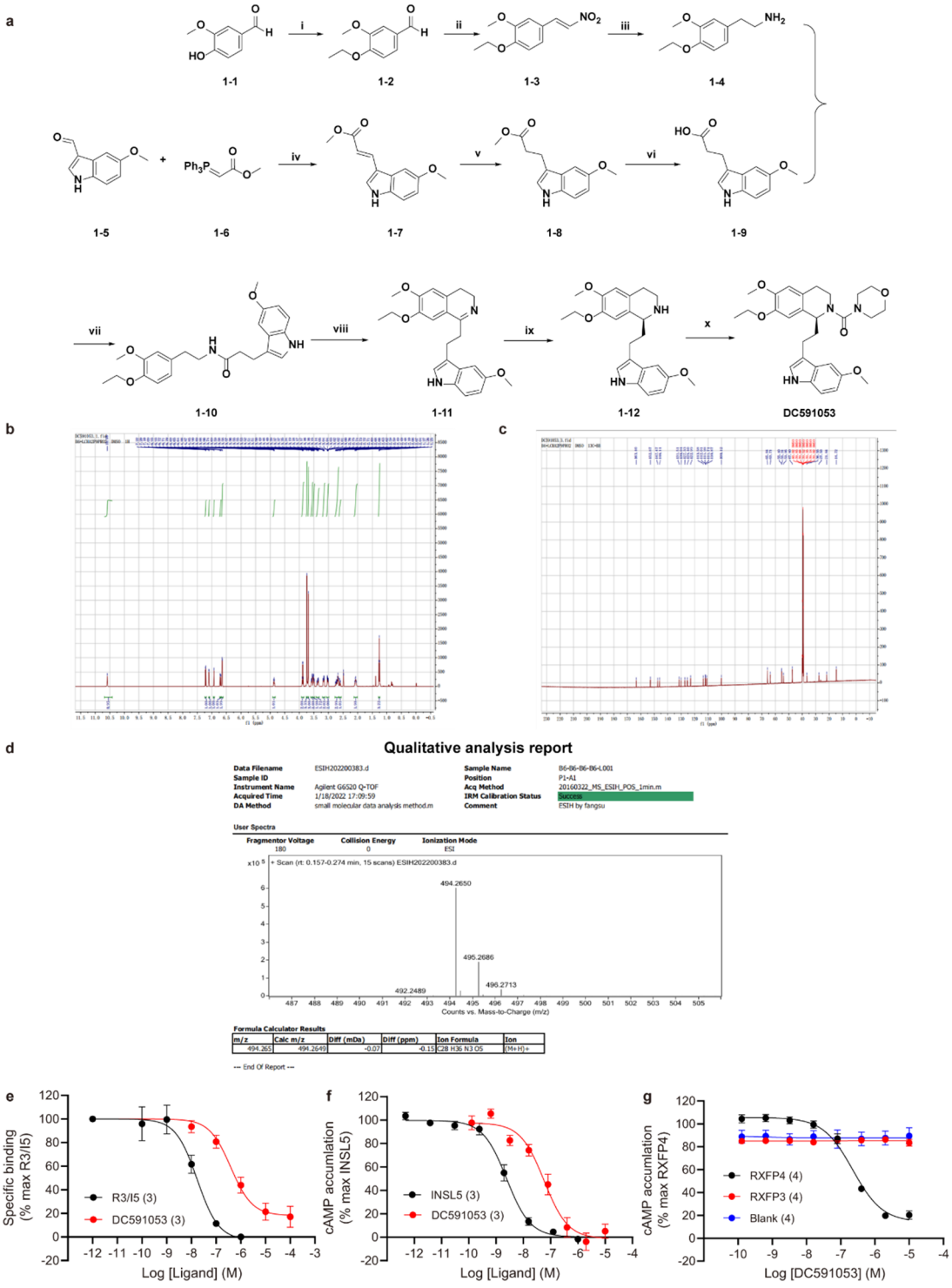


**Supplementary Figure 2. Synthesis and characterization of DC591053. a,** Synthetic route to the compound DC591053. (i) $CH_3CH_2I$, $CH_3CN$, $K_2CO_3$, 80 °C, Ar, 90%; (ii) $CH_3COONH_4$, $CH_3NO_2$, 100 °C ,1 h, 65%; (iii) $LiAlH_4$, anhydrous THF, 0 - rt, Ar, 78%; (iv) Toluene, Ar, 110 °C, 16 h, 60%; (v) 10% $Pd(OH)_2/C$, $H_2$, MeOH, 40 °C, 5 h, 95%; (vi) 1M NaOH, MeOH, rt, 93%; (vii) HATU, TEA, rt, DCM, 90%; (viii) $POCl_3$, $CH_3CN$, 80 °C, Ar, 92%; (ix) RuCl[(*R,R*)-Tsdpen](*p*-cymene), $AgSbF_6$, $La(OTf)_3$, HCOONa, $H_2O$/MeOH= 1:1, Ar, rt, 60%; (x) 4-morpholinecarbonyl chloride,

DIPEA, DCM, 0 °C to rt, 90%. **b,** $^{1}$H NMR spectrum of compound DC591053 (500 MHz, DMSO-$d_6$). **c,** $^{13}$C NMR spectrum of compound DC591053 (125 MHz, DMSO-$d_6$). **d,** HRMS spectrum of compound DC591053**. e-f,** DC591053 was able to bind and activate RXFP4 as determined by europium-labeled ligand competitive binding **(e)** and cAMP accumulation assays **(f).** Data shown are means ± S.E.M. of three independent experiments labeled in the parentheses. **g,** DC591053 neither cross-reacted with RXFP3 nor showed any activity in parental cells. Data shown are means ± S.E.M. of four independent experiments labeled in the parentheses. Source data are provided as a Source Data file.

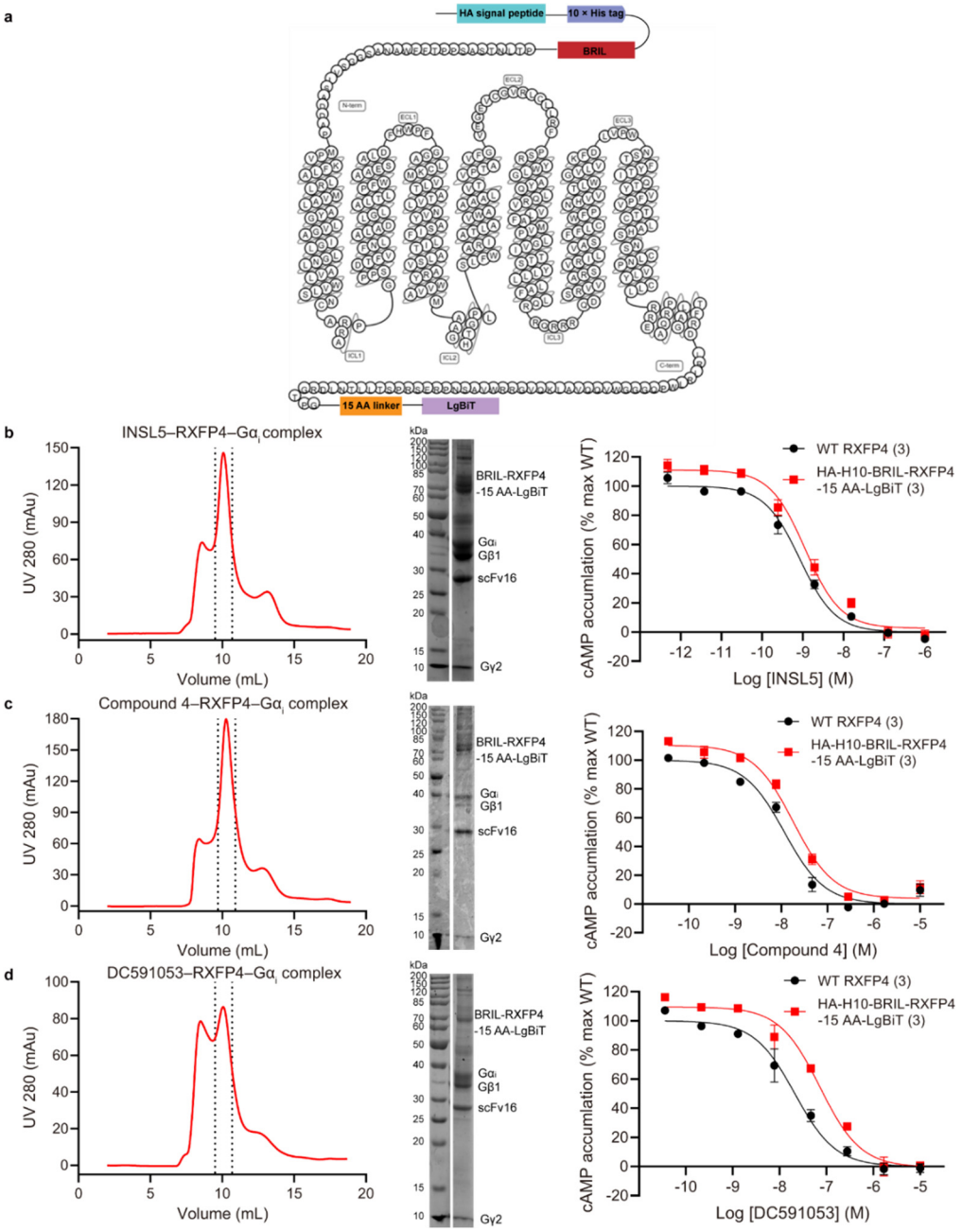


**Supplementary Figure 3. Functional validations of the receptor constructs and purification of the complexes. a,** Schematic diagram of the receptor constructs used for structure determination. **b-d,** Analytical size-exclusion chromatography (left) and SDS-PAGE/Coomassie blue stain (middle) of the purified INSL5–RXFP4–$G_i$ **(b)**, Compound 4–RXFP4–$G_i$ **(c)** and DC591053–RXFP4–$G_i$ **(d)**. These experiments were repeated independently three times with similar results. The right panel in **b-d** is INSL5, compound 4 and DC591053 induced cAMP accumulation in wild-type (WT) and modified RXFP4 constructs. Data shown were means ± S.E.M. from three independent experiments shown in the parentheses. Supplementary Tables 3 provides detailed statistical evaluation such as *P* values and numbers of independent experiments (*n*). Source data are provided as a Source Data file.

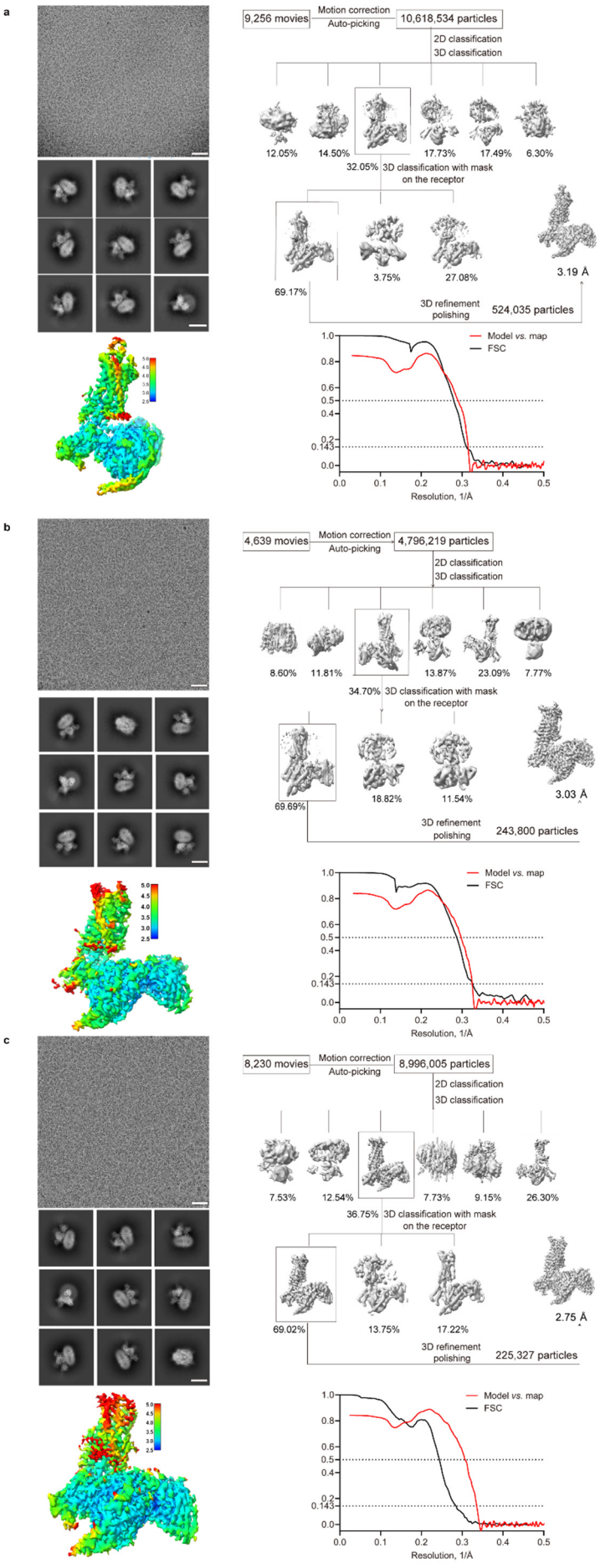
a
9,256 movies
Motion correction
Auto-picking
10,618,534 particles
2D classification
3D classification
12.05%
14.50%
32.05%
17.73%
17.49%
6.30%
3D classification with mask
on the receptor
69.17%
3.75%
27.08%
3.19 Å
3D refinement
polishing
524,035 particles
Model vs. map
FSC
Resolution, 1/Å
b
4,639 movies
Motion correction
Auto-picking
4,796,219 particles
2D classification
3D classification
8.60%
11.81%
34.70%
13.87%
23.09%
7.77%
3D classification with mask
on the receptor
69.69%
18.82%
11.54%
3.03 Å
3D refinement
polishing
243,800 particles
Model vs. map
FSC
Resolution, 1/Å
c
8,230 movies
Motion correction
Auto-picking
8,996,005 particles
2D classification
3D classification
7.53%
12.54%
36.75%
7.73%
9.15%
26.30%
3D classification with mask
on the receptor
69.02%
13.75%
17.22%
2.75 Å
3D refinement
polishing
225,327 particles
Model vs. map
FSC
Resolution, 1/Å

**Supplementary Figure 4. Cryo-EM data processing and validation. a,** INSL5–RXFP4–$G_i$ complex: top left, representative cryo-EM micrograph (scale bar: 40 nm) and two-dimensional (2D) class averages showing distinct secondary structure features from different views (scale bar: 5 nm); top right, flow chart of cryo-EM data processing; bottom left, local resolution distribution map of the complex; bottom right, Fourier shell correlation (FSC) curves of overall refined receptor. **b,** Compound 4–RXFP4–$G_i$ complex: top left, representative cryo-EM micrograph (scale bar: 40 nm) and 2D class averages showing distinct secondary structure features from different views (scale bar: 5 nm); top right, flow chart of cryo-EM data processing; bottom left, local resolution distribution map of the complex; bottom right, FSC curves of overall refined receptor. **c,** DC591053–RXFP4–$G_i$ complex top left, representative cryo-EM micrograph (scale bar: 40 nm) and 2D class averages showing distinct secondary structure features from different views (scale bar: 5 nm); top right, flow chart of cryo-EM data processing; bottom left, local resolution distribution map of the complex; bottom right, FSC curves of overall refined receptor. These experiments were repeated twice independently with similar results. Source data are provided as a Source Data file.

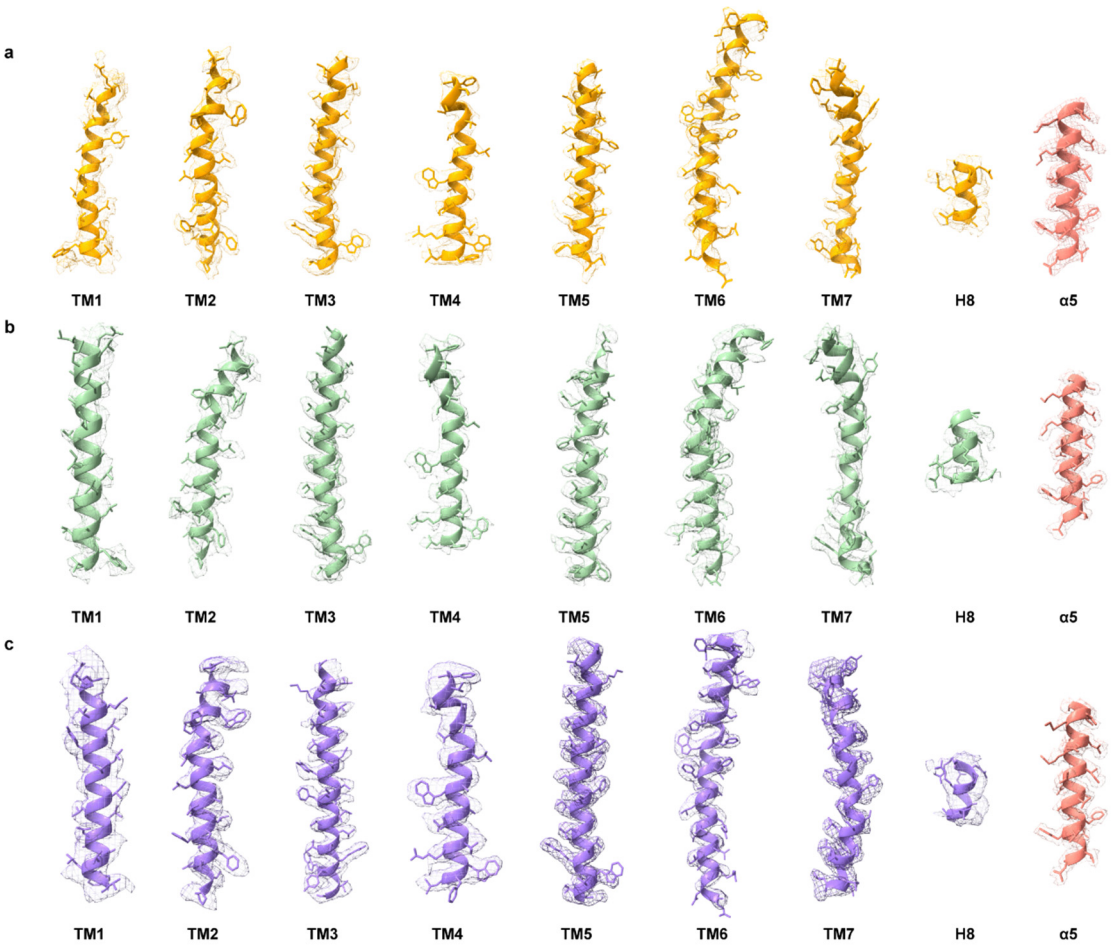


**Supplementary Figure 5. Near-atomic resolution model of the complexes in the cryo-EM density maps. a,** EM density map and model of the INSL5–RXFP4–$G_i$ complex are shown for all seven-transmembrane (7TM) α-helices, helix 8 and the α5-helix of the $G_i$ subunit. The receptor and α5-helix of the $G_i$ subunit are colored by orange and salmon, respectively. **b,** EM density map and model of the compound 4–RXFP4–$G_i$ complex are shown for all 7TM α-helices, helix 8 and the α5-helix of the $G_i$ subunit. The receptor and α5-helix of the $G_i$ subunit are colored by dark sea green and salmon, respectively. **c,** EM density map and model of the DC591053–RXFP4–$G_i$ complex are shown for all 7TM α-helices, helix 8 and the α5-helix of the $G_i$ subunit. The receptor and α5-helix of the $G_i$ subunit are colored by medium purple and salmon, respectively.

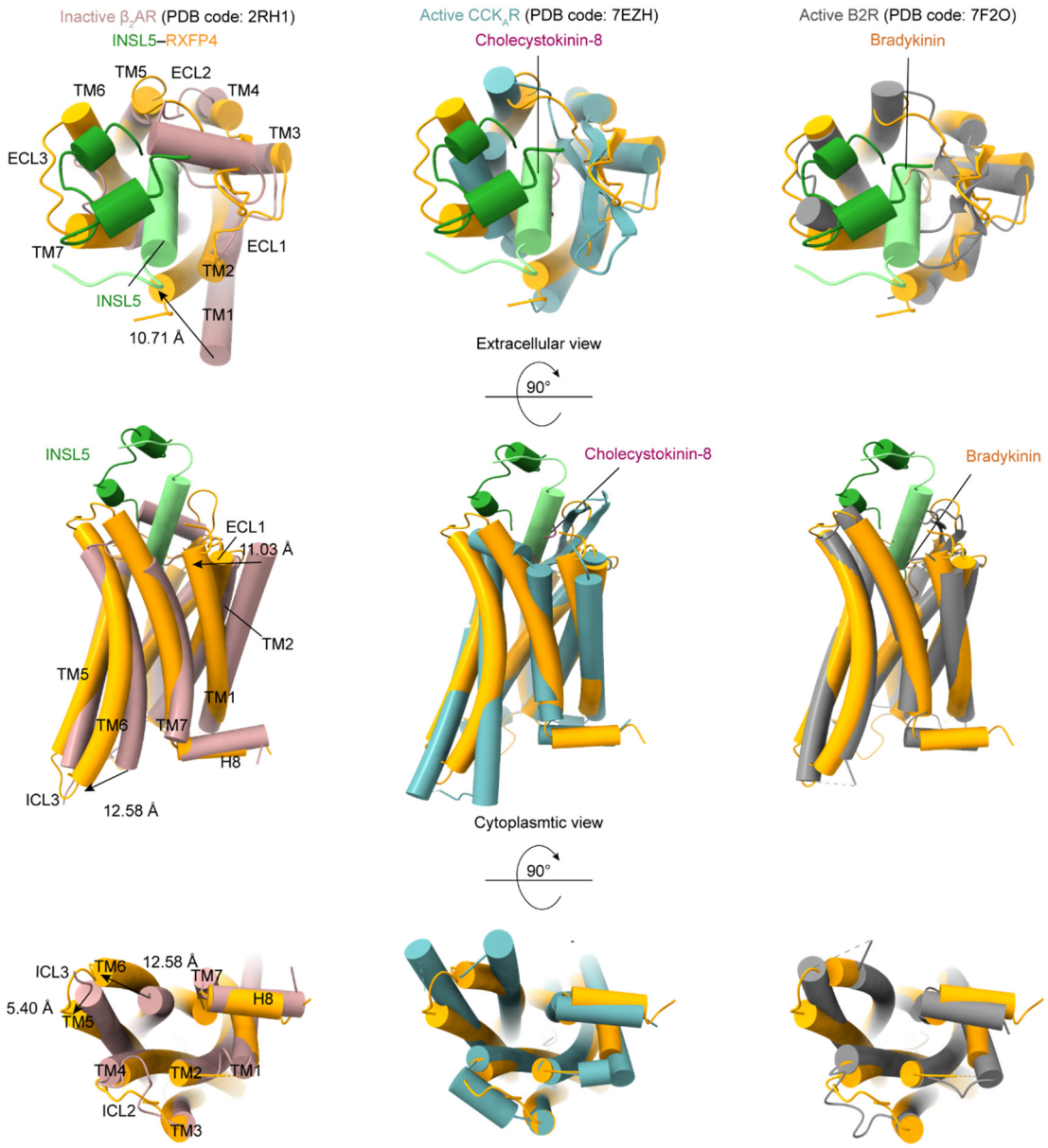


**Supplementary Figure 6. Conformational changes upon RXFP4 activation**. Comparison of active RXFP4 (orange) with inactive $\beta_2$-adrenergic receptor ($\beta_2$AR) (rosy brown, PDB code: 2RH1)[1] and both agonist-bound and G protein-coupled active cholecystokinin A receptor ($CCK_AR$) (cadet blue, PDB code: 7EZH)[2] and type 2 bradykinin receptor (B2R) (gray, PDB code: 7F2O)[3]. G proteins were omitted for clarity.


**Supplementary Figure 7. Comparison of the peptide-binding pocket of RXFP4 with other class A GPCRs.** The binding cavity of INSL5, compound 4 and DC591053-bound RXFP4 (**a**) were compared with that of other GPCRs **(b-g)** including small molecule bound receptors [adenosine in adenosine $A_1$ receptor ($A_1R$) (PDB code: 7LD4) and bromocriptine in D2 dopamine receptors (DRD2) (PDB code: 7JVR)] **(b)**, glucagon-like peptide-1 (GLP-1)-bound glucagon-like peptide-1 receptor (GLP-1R) (PDB code: 6X18) **(c)**, the N terminus of peptides inserts into the TMD core such as DAMGO-bound μ-opioid receptor (μOR) (PDB code: 6DDE), C-C chemokine ligand 15 [CCL15(26-92)]-bound C-C chemokine receptor type 1 (CCR1) (PDB code: 7VL9), C-X-C motif chemokine ligand 8 (CXCL8)-bound C-X-C chemokine receptor type 2 (CXCR2) (PDB code: 6LFO), $Aβ_{42}$-bound formyl peptide receptor 2 (FPR2) (PDB code: 7WVY), *N*-formyl humanin-bound FPR2 (PDB code: 7WVX) and ghrelin-bound growth hormone secretagogue receptor (GHSR) (PDB code: 7NA7) **(d)**, the middle segment of cyclic peptides inserts into the TMD binding cavity

such as α-melanocyte-stimulating hormone (α-MSH)-bound melanocortin 1 receptor (MC1R) (PDB code: 7F4D), somatostain-14-bound somatostatin receptor 2 (SSTR2) (PDB code: 7T10) and arginine-vasopressin (AVP)-bound vasopressin receptor 2 (V2R) (PDB code: 7DW9) **(e)**, the C terminus of peptides inserts into the TMD binding pocket such as angiotensin II-bound angiotensin II receptor type 1 (AT1R) (PDB code: 6OS0) and angiotensin II receptor type 2 (AT2R) (PDB code: 6JOD), Des-Arg10-kallidin bound (type 1 bradykinin receptor) B1R (PDB code: 7EIB), bradykinin-bound B2R (PDB code: 7F2O), cholecystokinin-8 (CCK-8)-bound $CCK_AR$ (PDB code: 7EZH) and gastrin-17 bound cholecystokinin B receptor ($CCK_BR$) (PDB code: 7F8V), JMV449-bound neurotensin receptor 1 (NTSR1) (PDB code: 6OS9), neuromedin U-bound neuromedin U receptor 2 (NUM2R) (PDB code: 7W55) and neuromedin S-bound NUM2R (PDB code: 7W57) **(f)**, and unique binding mode of galanin with galanin receptor 1 (GAL1R) (PDB code: 7WQ3) and galanin receptor 2 (GAL2R) (PDB code: 7WQ4) **(g).**

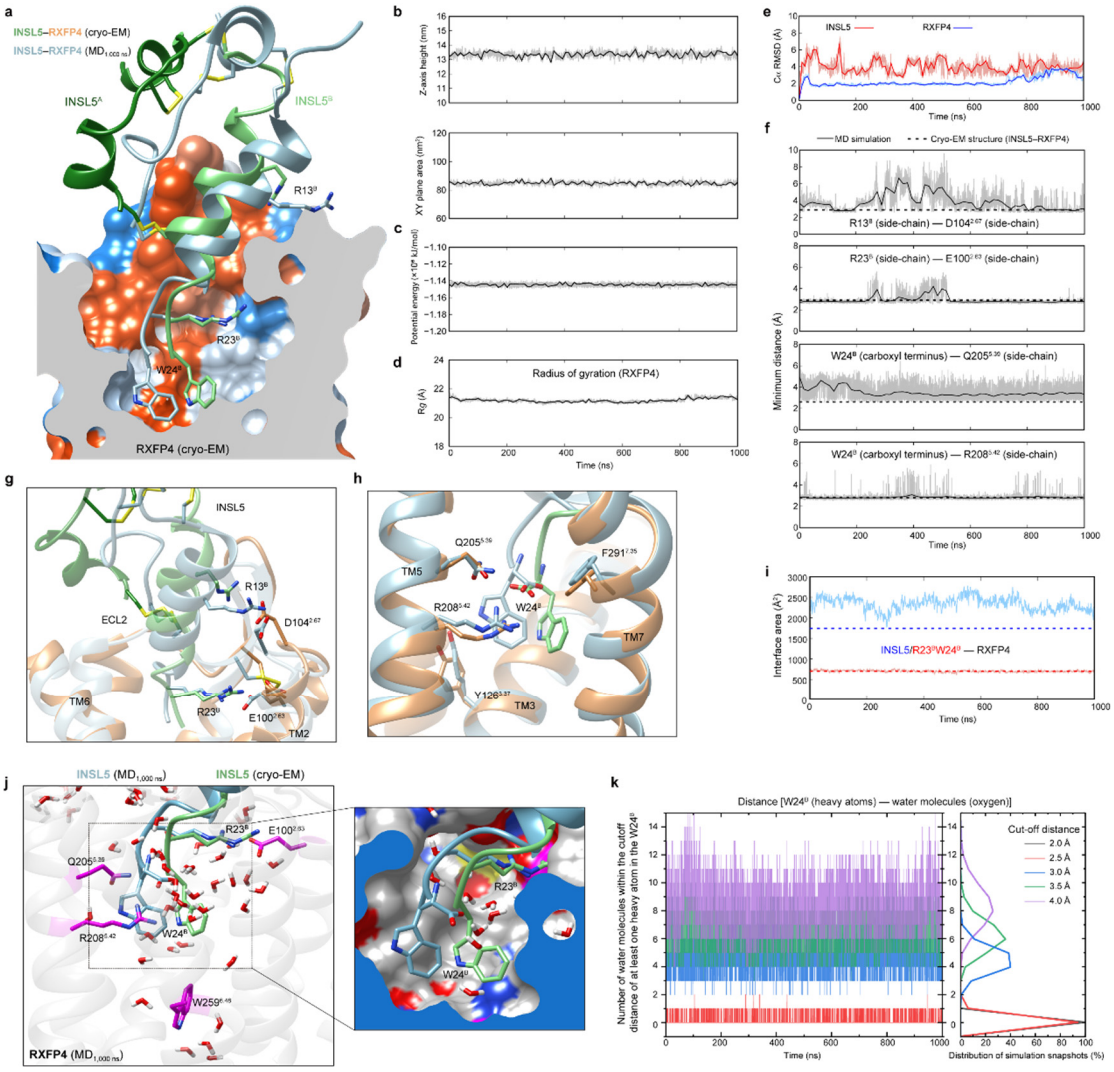


**Supplementary Figure 8. Molecular dynamics (MD) simulations of INSL5-bound active RXFP4. a,** Comparison of the INSL5 conformation between the final simulation snapshot at 1,000 ns and the cryo-EM structure of INSL5–RXFP4–$G_i$ complex. The key residues in the peptide-receptor interface are shown in sticks. **b,** Time evolution of the Z-axis height (top) and XY plane area (bottom) of the simulation box during MD simulation. **c,** Potential energy fluctuation during MD simulation. **d,** Radius of gyration (R*g*) of RXFP4 during MD simulation. **e,** Root mean squared deviation (RMSD) of Cα positions of the RXFP4 and INSL5, where all snapshots were superimposed on the cryo-EM structure of RXFP4 and INSL5 using the Cα atoms, respectively. **f-h,** Close-up views of the interactions between the C terminal α-helix of INSL5 B chain and receptor residues (**g** and **h**) and their minimum distances during MD simulations (**f**). **i,** The interface area

between RXFP4 and INSL5 (blue) or the two C terminus residues $R23^{B}$ and $W24^{B}$ (red), calculated by FreeSASA 2.0. The thick and thin traces represent moving averages and original, unsmoothed values obtained from one single MD simulation trajectory, respectively. **j,** The distribution of water molecules in the orthosteric pocket that overlap with the position of indole group of $W24^{B}$ in the cryo-EM structure model (green). A close-up view of the internal water molecules distributed around the C terminus of the INSL5 B chain was shown on the right. **k,** Time evolution of the number of water molecules within the cut-off distance of $W24^{B}$ during MD simulation. Only these water molecules whose oxygen atoms located within the cut-off distance of at least one heavy atom in the $W24^{B}$ were counted. Five cut-off distances (2.0 Å, 2.5 Å, 3.0 Å, 3.5 Å, and 4.0 Å) were adopted. The MD simulations were repeated independently three times with similar results.

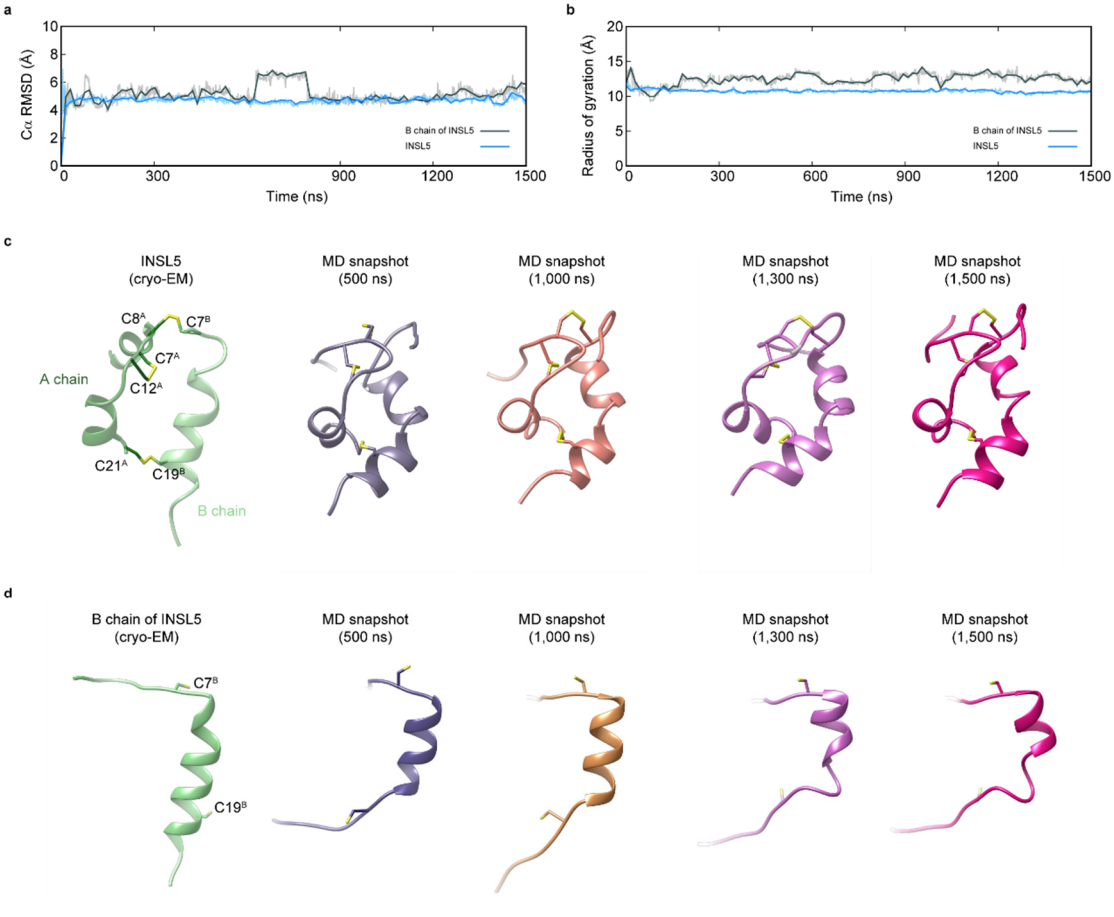


**Supplementary Figure 9. MD simulations of INSL5 and its B chain. a,** RMSD of Cα positions of the INSL5 and its B chain, where all snapshots were superimposed on the cryo-EM structure of INSL5 and its B chain using the Cα atoms, respectively. **b,** Radius of gyration of non-hydrogen atoms of the INSL5 and its B chain during MD simulations. **c,** Representative snapshots of MD simulations of INSL5. The cysteines are shown in sticks. **d,** Representative snapshots of MD simulations of the B chain of INSL5. The cysteines are shown in sticks. The thick and thin traces represent moving averages and original, unsmoothed values obtained from one single MD simulation trajectory, respectively. The MD simulations were repeated independently three times with similar results.

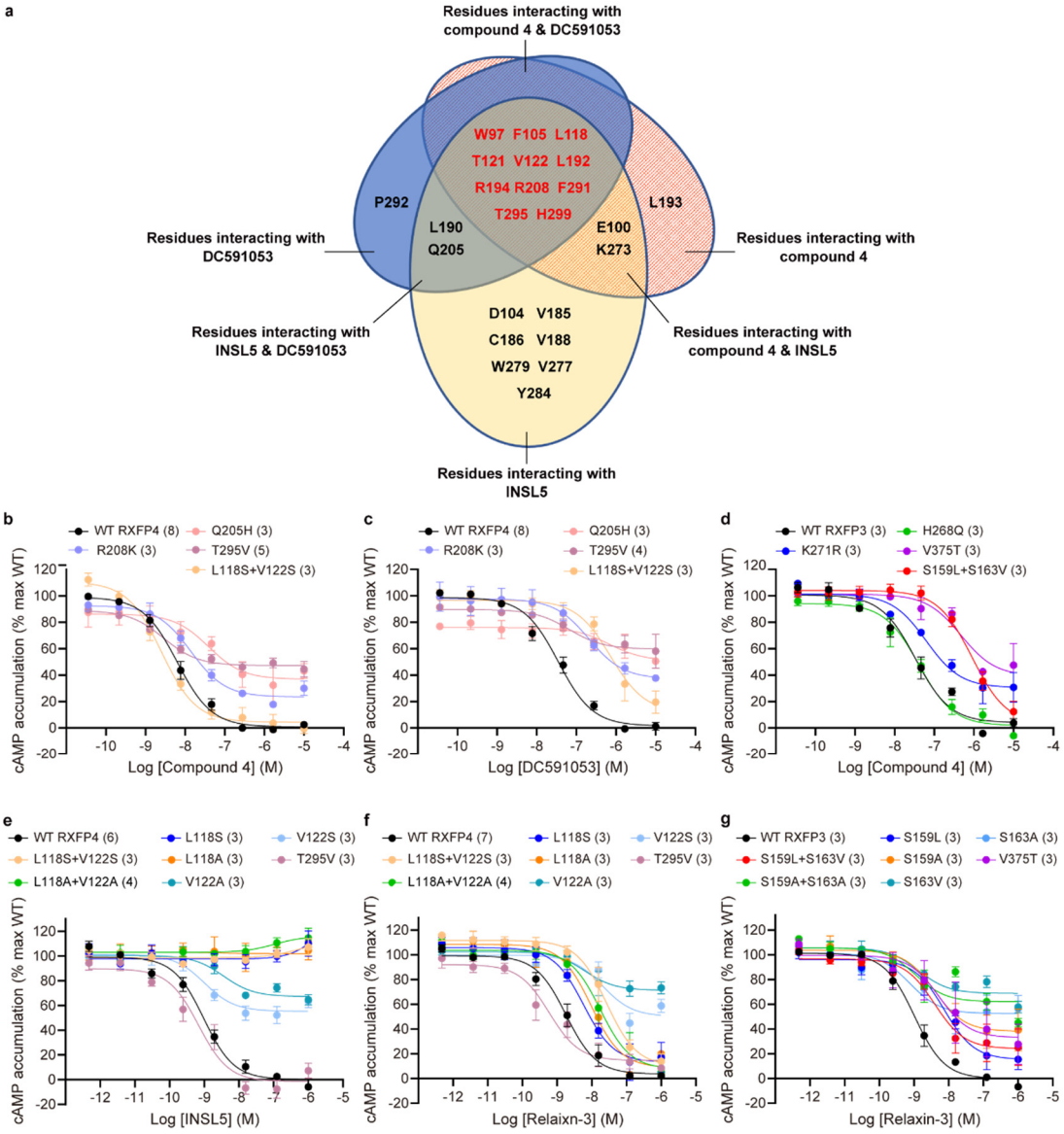


**Supplementary Figure 10. Peptidomimetic agonism and key residues on receptor subtype selectivity. a,** RXFP4 residues are categorized according to their interactions with the three ligands. **b-d,** Effects of amino acid switch in equivalent positions between RXFP4 and RXFP3 around the ligand-binding pocket on compound 4 **(b)** and DC591053 **(c)** induced cAMP accumulation in RXFP4 as well as on compound 4 induced cAMP accumulation in RXFP3 **(d)**. **e-f,** Effects of INSL5 **(e)** and relaxin-3 **(f)** on cAMP accumulation in WT and mutant RXFP4s. **g,** Effects of relaxin-3 on cAMP accumulation in WT and mutant RXFP3. INSL5 was totally inactive in RXFP4 single mutants L118$^{3.29}$S and L118$^{3.29}$A as well as double mutants L118$^{3.29}$S+V122$^{3.33}$S and L118$^{3.29}$A+V122$^{3.33}$A, where relaxin-3 retained partial activity although the curves shifted to the right (by 3.2-fold, 5.4-fold, 21.8-fold and 9.7-fold, respectively). For comparison, relaxin-3 activated S159$^{3.29}$A, S159$^{3.29}$L, S159$^{3.29}$L+S163$^{3.33}$V and S159$^{3.29}$A+S163$^{3.33}$A in RXFP3 albeit with reduced potencies. T295$^{7.39}$V did not destroy the response of RXFP4 to INSL5 and relaxin-3, but

V375$^{7.39}$T in RXFP3 impaired both the potency (by 5.1-fold) and $E_{max}$ (66.5% of the WT) of relaxin-3 (INSL5 was inactive in WT and all the five RXFP3 mutants). Therefore, S159$^{3.29}$, S163$^{3.33}$ and V375$^{7.39}$ in RXFP3 and L118$^{3.29}$, V122$^{3.33}$ and T295$^{7.39}$ in RXFP4 are likely involved in RXFP3 *vs.* RXFP4 subtype selectivity, consistent with the observations in RXFP3/RXFP4 chimeric receptor studies[4]. Data were shown as means ± S.E.M. of at least three independent experiments. The numbers of independent experiments are shown in the parentheses. Supplementary Tables 4 and 5 provide detailed statistical evaluation such as *P* values and numbers of independent experiments (*n*). Source data are provided as a Source Data file.

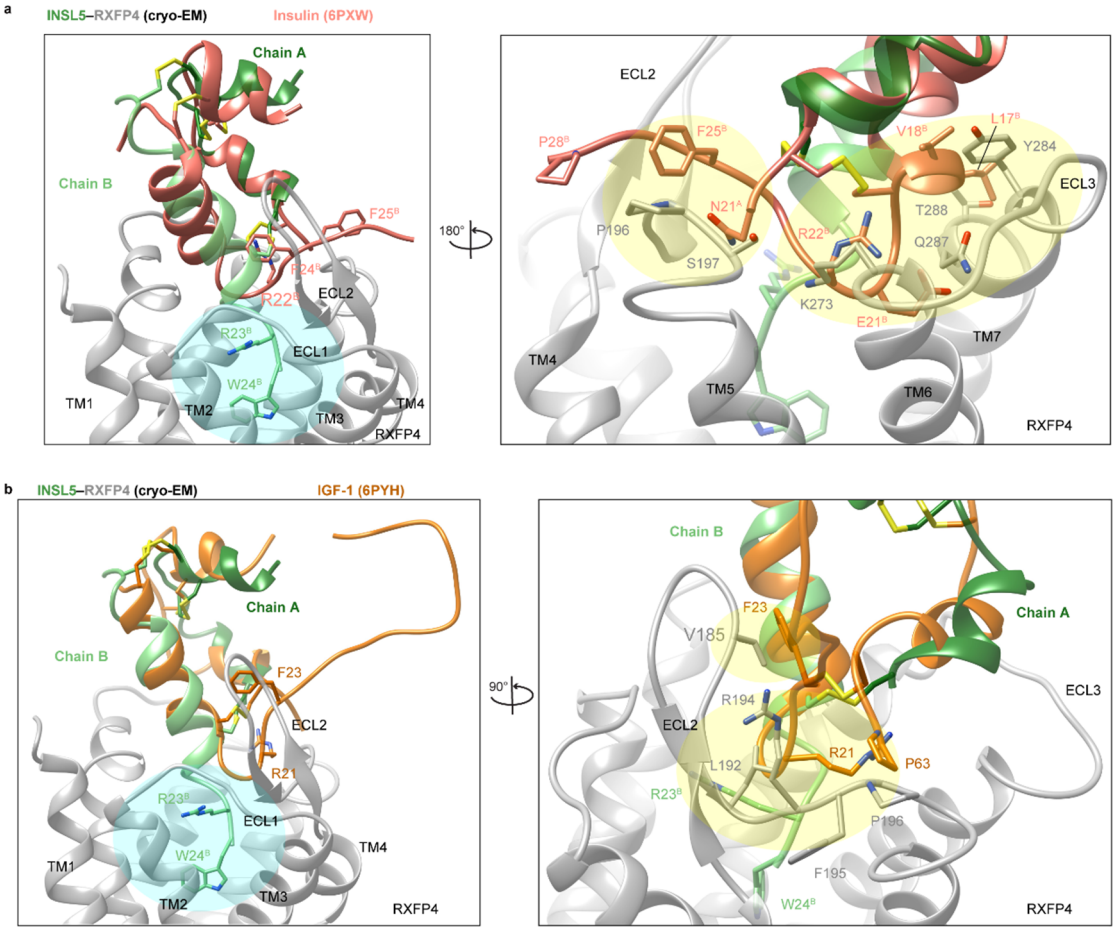


**Supplementary Figure 11. Superimposition of INSL5 from the INSL5–RXFP4–$G_i$ complex structure with insulin or IGF-1. a,** Insulin (salmon, PDB code: 6PXW) was superimposed on the INSL5 (green) from the cryo-EM structure of INSL5–RXFP4–$G_i$ using the Cα atoms. The three disulfide bonds and key residues in the peptide-receptor interface are shown in sticks. Compared to the endogenous agonist INSL5, the aligned insulin loses multiple potent interactions (cyan-shaded region) and causes significant steric clashes (yellow-shaded region) with RXFP4 (gray). **b,** IGF-1 (orange, PDB code: 6PYH) was superimposed on the INSL5 (green) from the cryo-EM structure of INSL5–RXFP4–$G_i$ using the Cα atoms. Compared to the endogenous agonist INSL5, the aligned IGF-1 loses multiple potent interactions (cyan-shaded region) and causes significant steric clashes (yellow-shaded region) with RXFP4 (gray).

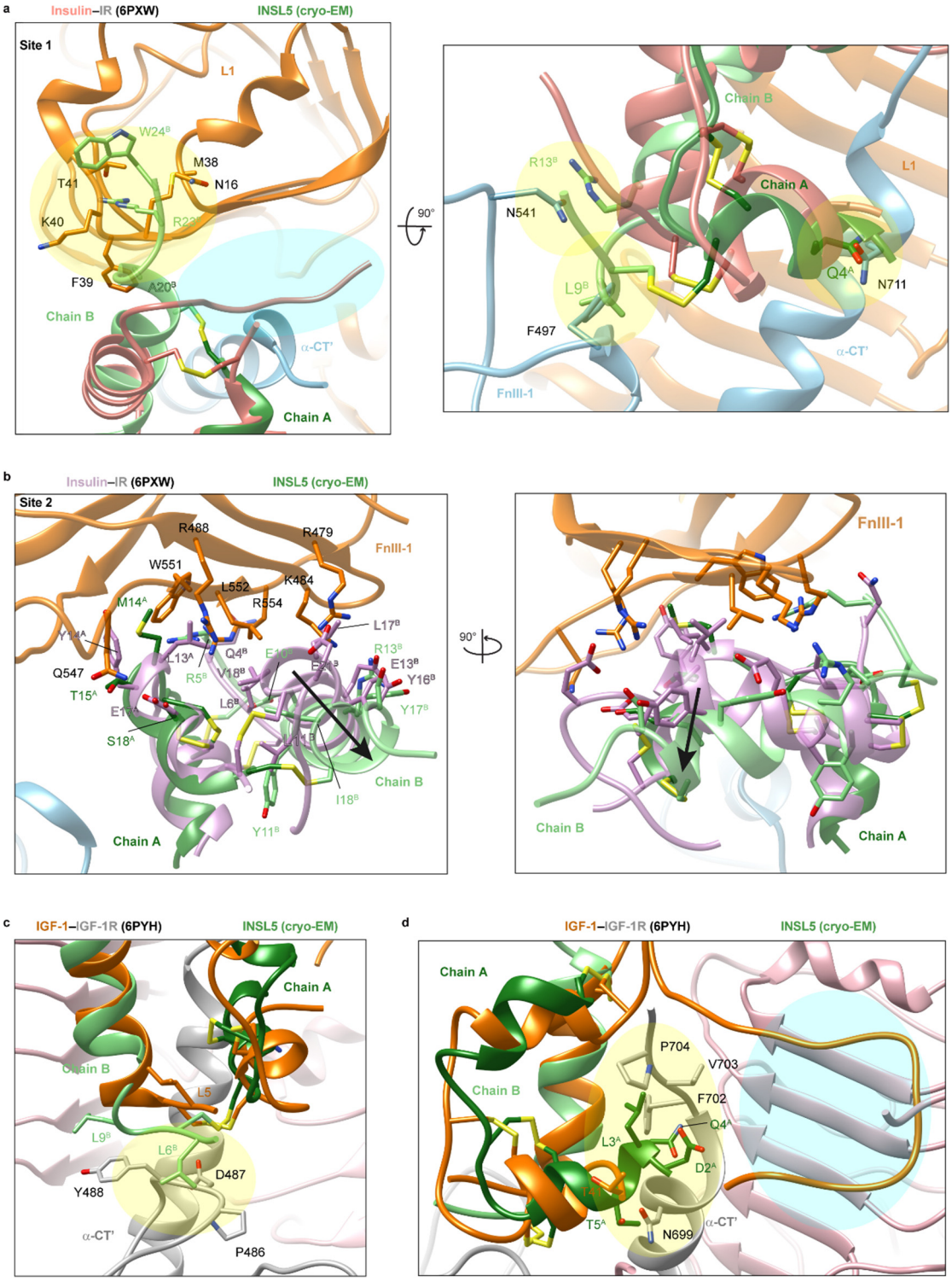


**Supplementary Figure 12. Superimposition of INSL5 to insulin or IGF-1 in complex with cognate receptors. a-b,** INSL5 (green) was superimposed on the insulin at site 1 (salmon, **a**) or at site 2 (plum, **b**) from the cryo-EM structure of insulin–insulin receptor (PDB code: 6PXW) using the Cα atoms. The three disulfide bonds and key residues in the peptide-receptor interface are shown in sticks. Compared to the endogenous agonist insulin, the aligned INSL5 loses multiple potent interactions (cyan-shaded region) and causes significant steric clashes (yellow-shaded region) with

insulin receptor. **c,** INSL5 (green) was superimposed on the IGF-1 (orange) from the cryo-EM structure of IGF-1–IGF-1R (PDB code: 6PYH) using the Cα atoms. The three disulfide bonds and key residues in the peptide-receptor interface are shown in sticks. **d,** Compared to the endogenous agonist IGF-1, the aligned INSL5 loses multiple potent interactions (cyan-shaded region) and causes significant steric clashes (yellow-shaded region) with IGF-1R.

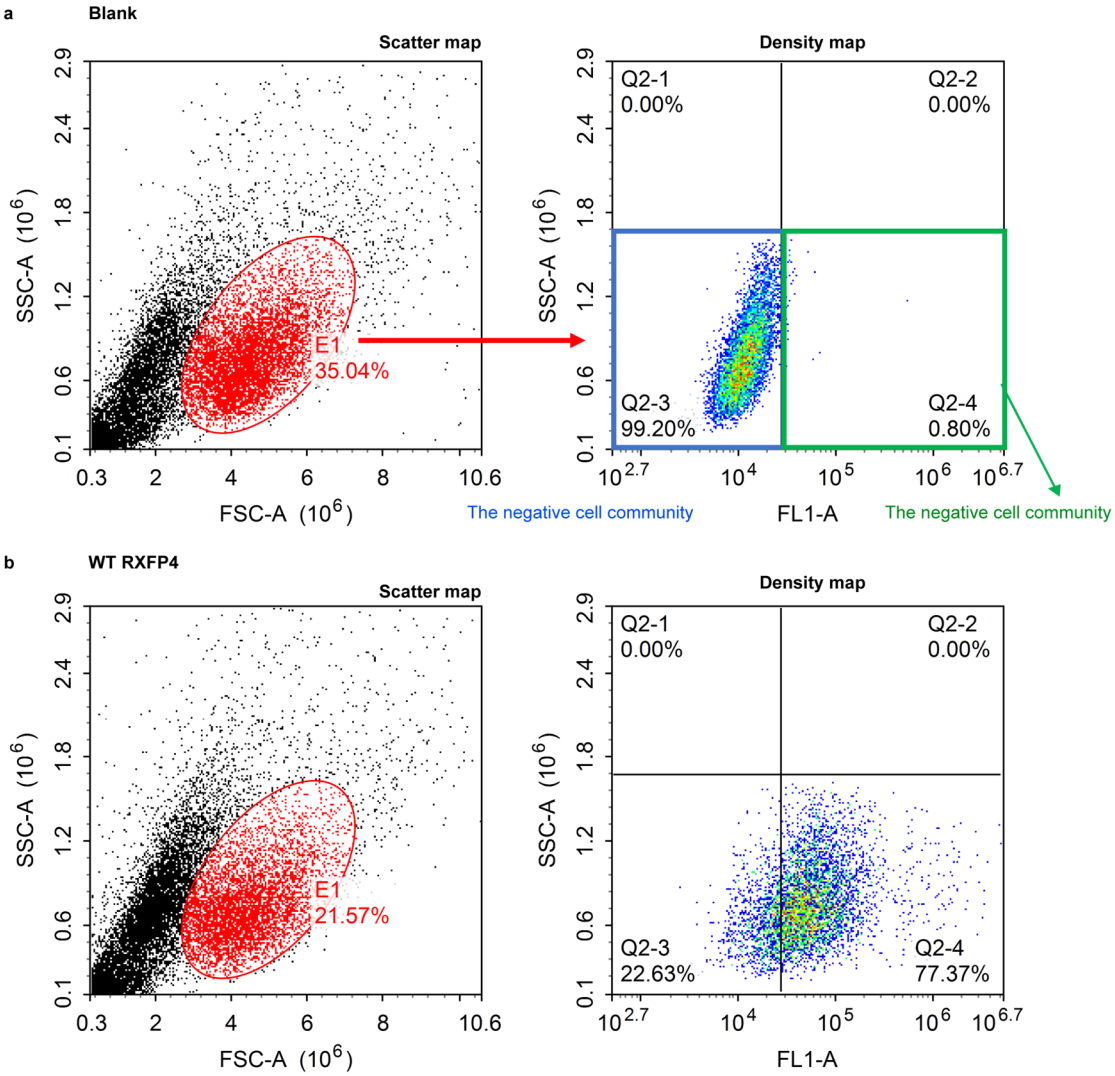


**Supplementary Figure 13. Gating strategy of the cell surface expression assay.** Circle a gate E1 in the scatter map (red circle) and the cells shown in the density map are all the cells in the gate E1 of the scatter map. Fluorescence signal intensity (FITC) is presented by density map. With the blank sample (no receptor transfection) as the reference value of background fluorescence signal (**a**), the "quadrant gate" divides the fluorescence signal density map into four quadrants. The third quadrant represents the negative cell community, while the fourth quadrant represents the positive cell community. The expression value of wild-type (WT) receptor (**b**) can be calculated as follows: (M(Q2-4)-M(Q2-3)) × (Q2-4% Parent). The calculation of receptor mutants is the same as that of the WT receptor, which was then normalized with the WT receptor to calculate the relative expression value of the mutants.

**Supplementary Table 1** Cryo-EM data collection, refinement and validation statistics.

| | **INSL5–RXFP4 (1-374)–$G_i$** | **Compound 4–RXFP4 (1-374)–$G_i$** | **DC591053–RXFP4 (1-374)–$G_i$** |
|---|---|---|---|
| **Data collection and processing** | | | |
| Magnification | 46,685 | 46,685 | 46,685 |
| Voltage (kV) | 300 | 300 | 300 |
| Electron exposure ($e^{-}$/Å$^2$) | 80 | 80 | 80 |
| Defocus range (μm) | -1.2 to -2.2 | -1.2 to -2.2 | -1.2 to -2.2 |
| Pixel size (Å) | 1.071 | 1.071 | 1.071 |
| Symmetry imposed | Cl | Cl | Cl |
| Initial particle images (no.) | 10,618,534 | 4,796,219 | 8,996,005 |
| Final particle images (no.) | 524,035 | 243,800 | 225,327 |
| Map resolution (Å) | 3.19 | 3.03 | 2.75 |
| FSC threshold | 0.143 | 0.143 | 0.143 |
| Map resolution range (Å) | 2.5-5.0 | 2.5-5.0 | 2.5-5.0 |
| **Refinement** | | | |
| Initial model used (PDB code) | PDB codes 7F2O and 6D9H | PDB codes 7F2O and 6D9H | PDB codes 7F2O and 6D9H |
| Model resolution (Å) | 3.3 | 3.2 | 3.1 |
| FSC threshold | 0.5 | 0.5 | 0.5 |
| Model resolution range (Å) | 2.5-5.0 | 2.5-5.0 | 2.5-5.0 |
| Map sharpening B factor (Å$^2$) | -163.30 | -96.90 | -106.50 |
| Model composition | | | |
| Non-hydrogen atoms | 8980 | 8731 | 8761 |
| Protein residues | 1154 | 1118 | 1122 |
| B factors (Å$^2$) | | | |
| Protein | 93.61 | 80.83 | 78.02 |
| Ligand | — | 70.68 | 77.67 |
| R.m.s. deviations | | | |
| Bond lengths (Å) | 0.004 | 0.004 | 0.004 |
| Bond angles (°) | 0.599 | 0.552 | 0.666 |
| Validation | | | |
| MolProbity score | 1.84 | 1.69 | 1.79 |

| | | | |
|---|---|---|---|
| Clash score | 9.24 | 8.75 | 8.03 |
| Poor rotamers (%) | 0.00 | 0.00 | 0.00 |
| Ramachandran plot | | | |
| Favored (%) | 94.96 | 96.61 | 94.98 |
| Allowed (%) | 5.04 | 3.39 | 5.02 |
| Disallowed (%) | 0.00 | 0.00 | 0.00 |
| Rama-Z score | 0.71 | 0.16 | 0.78 |

**Supplementary Table 2** Interactions of INSL5, compound 4 and DC591053 with RXFP4.

| RXFP4 | INSL5 | Compound 4 | DC591053 |
|---|---|---|---|
| W97$^{2.60}$ | Stacking | Stacking | Stacking |
| E100$^{2.63}$ | Salt bridge | Salt bridge | —— |
| D104$^{2.67}$ | Hydrogen bond | —— | —— |
| F105$^{ECL1}$ | Stacking | Stacking | Stacking |
| L118$^{3.29}$ | Hydrophobic contact | Hydrophobic contact | Hydrophobic contact |
| T121$^{3.32}$ | Hydrogen bond | Hydrophobic contact | Hydrophobic contact |
| V122$^{3.33}$ | Hydrophobic contact | Hydrophobic contact | Hydrophobic contact |
| V185$^{ECL2}$ | Hydrophobic contact | —— | —— |
| C186$^{ECL}$ | Hydrophobic contact | —— | —— |
| V188$^{ECL2}$ | Hydrophobic contact | —— | —— |
| L190$^{ECL2}$ | Hydrophobic contact | —— | Hydrophobic contact |
| L192$^{45.51}$ | Hydrophobic contact | Hydrophobic contact | Hydrophobic contact |
| L193$^{45.52}$ | —— | Hydrophobic contact<br>Hydrogen bond | —— |
| R194$^{ECL2}$ | Weak hydrogen bond | Hydrogen bond | Stacking |
| Q205$^{5.39}$ | Hydrogen bond | —— | Hydrogen bond |
| R208$^{5.42}$ | Salt bridge<br>Stacking | Stacking | Hydrogen bond<br>Stacking |
| K273$^{6.62}$ | Salt bridge<br>Hydrophobic contact | Hydrogen bond | —— |
| V277$^{ECL3}$ | Hydrophobic contact | —— | —— |
| W279$^{ECL3}$ | Hydrophobic contact | —— | —— |
| Y284$^{7.28}$ | Hydrophobic contact | —— | —— |
| F291$^{7.35}$ | Stacking | Stacking | Stacking |
| P292$^{7.36}$ | —— | —— | Hydrophobic contact |
| T295$^{7.39}$ | Hydrophobic contact | Hydrogen bond | Hydrogen bond |
| H299$^{7.43}$ | Stacking | Hydrogen bond | Stacking |

**Supplementary Table 3.** Ligand-mediated inhibition of forskolin-induced cAMP accumulation.

| Receptor | INSL5 | | | | | Compound 4 | | | | | DC591053 | | | | |
|---|---|---|---|---|---|---|---|---|---|---|---|---|---|---|---|
| | $pEC_{50}$ | | $E_{max}$ (% WT) | | *n* | $pEC_{50}$ | | $E_{max}$ (% WT) | | *n* | $pEC_{50}$ | | $E_{max}$ (% WT) | | *n* |
| | Means ± S.E.M. | *P* value | Means ± S.E.M. | *P* value | | Means ± S.E.M. | *P* value | Means ± S.E.M. | *P* value | | Means ± S.E.M. | *P* value | Means ± S.E.M. | *P* value | |
| WT RXFP4 | 9.07 ± 0.07 | — | 99.76 ± 2.15 | — | 3 | 7.94 ± 0.08 | — | 99.99 ± 2.85 | — | 3 | 7.68 ± 0.09 | — | 99.14 ± 2.97 | — | 3 |
| HA-H10-Bril-RXFP4 -15AA-LgBiT | 8.94 ± 0.08 | 0.8616 | 110.76 ± 2.64 | 0.7961 | 3 | 7.74 ± 0.07 | 0.8060 | 110.40 ± 2.36 | 0.8141 | 3 | 7.14 ± 0.08 | 0.8601 | 108.57 ± 2.51 | 0.8329 | 3 |

All data were fitted with a three-parameter logistic curve to obtain $pEC_{50}$ and $E_{max}$ values. The assay was performed in transiently transfected HEK293T cells. Data are presented as means ± S.E.M. of three independent experiments ($n = 3$) performed in quadruplicate. Statistical analysis was performed using a two-tailed Student's *t*-test and no significance was found among the values. The *P* value was defined as: **P*< 0.05, ***P*< 0.01, ****P*< 0.001 and *****P*< 0.0001. WT, wild-type.

**Supplementary Table 4.** Cell surface expression and effects of residue mutation on ligand-mediated inhibition of forskolin-induced cAMP accumulation.

| **Cell surface expression of receptor mutations** | | | | |
|---|---|---|---|---|
| **Receptor** | **Mutation** | **Cell surface expression (% WT)** | ***P* value** | ***n*** |
| RXFP4 | WT | 100 | —— | 7 |
| | W97A | 59.76 ± 0.21**** | <0.0001 | 3 |
| | E100A | 81.83 ± 4.56 | 0.1014 | 4 |
| | D104A | 38.82 ± 1.34**** | <0.0001 | 3 |
| | F105A | 69.26 ± 2.69** | 0.0016 | 3 |
| | T121A | 40.11 ± 2.25**** | <0.0001 | 3 |
| | R194A | 29.81 ± 1.01**** | <0.0001 | 3 |
| | Q205A | 80.26 ± 2.04 | 0.0569 | 4 |
| | R208A | 27.07 ± 1.09**** | <0.0001 | 3 |
| | K273A | 35.92 ± 2.69**** | <0.0001 | 3 |
| | W279A | 151.25 ± 6.66**** | <0.0001 | 5 |
| | Y284A | 123.5 ± 8.30** | 0.0059 | 5 |
| | H299A | 84.87 ± 8.49 | 0.1966 | 5 |
| | L118S+V122S | 24.79 ± 2.68**** | <0.0001 | 3 |
| | Q205H | 91.09 ± 1.43 | 0.8954 | 4 |
| | R208K | 68.61 ± 4.73**** | <0.0001 | 5 |
| | T295V | 66.15 ± 7.26**** | <0.0001 | 5 |
| RXFP3 | WT | 100 | —— | 3 |
| | S159L+S163V | 78.75 ± 2.54*** | 0.0003 | 3 |
| | H268Q | 96.03 ± 2.79 | 0.5787 | 3 |
| | K271R | 97.86 ± 1.15 | 0.9076 | 3 |
| | V375T | 95.63 ± 3.30 | 0.5022 | 3 |

| **Effects of residue mutation on INSL5-mediated inhibition of forskolin-induced cAMP accumulation** | | | | | | |
|---|---|---|---|---|---|---|
| **Receptor** | **Mutation** | ***p*EC$_{50}$** | | **E$_{max}$ (% WT)** | | ***n*** |
| | | **Mean ± S.E.M.** | ***P* value** | **Mean ± S.E.M.** | ***P* value** | |
| RXFP4 | WT | 9.12 ± 0.06 | —— | 99.88 ± 2.28 | —— | 6 |
| | W97A | 7.81 ± 0.18*** | 0.0008 | 61.33 ± 5.34**** | <0.0001 | 3 |
| | E100A | N.A. | —— | N.A. | —— | 3 |
| | D104A | 8.79 ± 0.25 | 0.8176 | 59.09 ± 6.41**** | <0.0001 | 3 |
| | F105A | 8.00 ± 0.11** | 0.0042 | 80.16 ± 4.08 | 0.0571 | 3 |
| | T121A | N.A. | —— | N.A. | —— | 4 |
| | R194A | 8.78 ± 0.17 | 0.7863 | 79.76 ± 6.06 | 0.0502 | 3 |
| | Q205A | 8.40 ± 0.30 | 0.1002 | 50.94 ± 6.54**** | <0.0001 | 3 |
| | R208A | N.A. | —— | N.A. | —— | 3 |
| | K273A | 8.45 ± 0.29 | 0.0940 | 58.10 ± 7.38**** | <0.0001 | 4 |

| | | | | | | |
|---|---|---|---|---|---|---|
| | W279A | 8.73 ± 0.17 | 0.6679 | 43.30 ± 3.29**** | <0.0001 | 3 |
| | Y284A | 8.74 ± 0.19 | 0.6174 | 49.25 ± 4.06**** | <0.0001 | 4 |
| | H299A | 9.02 ± 0.29 | 0.9994 | 30.77 ± 3.77**** | <0.0001 | 3 |
| **Effects of residue mutation on compound 4-mediated inhibition of forskolin-induced cAMP accumulation** | | | | | | |
| **Receptor** | **Mutation** | ***p*EC$_{50}$** | | **E$_{max}$ (% WT)** | | ***n*** |
| | | **Mean ± S.E.M.** | ***P* value** | **Mean ± S.E.M.** | ***P* value** | |
| RXFP4 | WT | 8.20 ± 0.07 | —— | 98.22 ± 3.01 | —— | 8 |
| | W97A | N.A. | —— | N.A. | —— | — |
| | E100A | N.A. | —— | N.A. | —— | — |
| | F105A | 7.81 ± 0.21 | 0.5144 | 60.11 ± 5.70**** | <0.0001 | 3 |
| | T121A | 6.90 ± 0.30**** | <0.0001 | 59.77 ± 8.29**** | <0.0001 | 3 |
| | R194A | 7.33 ± 0.24 ** | 0.0056 | 78.96 ± 8.75 | 0.0619 | 3 |
| | R208A | 7.38 ± 0.17** | 0.0094 | 63.76 ± 4.94*** | 0.0002 | 3 |
| | K273A | 7.33 ± 0.19** | 0.0056 | 76.06 ± 6.54* | 0.0227 | 3 |
| | H299A | N.A. | —— | N.A. | —— | 3 |
| | L118S+V122S | 8.60 ± 0.10 | 0.5000 | 106.23 ± 4.75 | 0.8663 | 3 |
| | Q205H | 7.41 ± 0.32* | 0.0135 | 49.35 ± 7.02**** | <0.0001 | 3 |
| | R208K | 7.85 ± 0.13 | 0.6570 | 69.09 ± 4.02** | 0.0016 | 3 |
| | T295V | 8.55 ± 0.15 | 0.4573 | 41.58 ± 2.93**** | <0.0001 | 5 |
| RXFP3 | WT | 7.48 ± 0.12 | —— | 96.70 ± 5.12 | —— | 3 |
| | S159L+S163V | 6.05 ± 0.12*** | 0.0006 | 101.29 ± 6.72 | 0.4990 | 3 |
| | H268Q | 7.39 ± 0.11 | 0.9792 | 92.52 ± 4.71 | 0.2208 | 3 |
| | K271R | 7.21 ± 0.17 | 0.8018 | 70.86 ± 5.48**** | <0.0001 | 3 |
| | V375T | 6.33 ± 0.24** | 0.0031 | 62.11 ±7.78**** | <0.0001 | 3 |
| **Effects of residue mutation on DC591053-mediated inhibition of forskolin-induced cAMP accumulation** | | | | | | |
| **Receptor** | **Mutation** | ***p*EC$_{50}$** | | **E$_{max}$ (% WT)** | | ***n*** |
| | | **Mean ± S.E.M.** | ***P* value** | **Mean ± S.E.M.** | ***P* value** | |
| RXFP4 | WT | 7.46 ± 0.07 | —— | 97.18 ± 3.11 | —— | 8 |
| | W97A | 7.25 ± 0.10 | 0.9961 | 108.65 ± 10.04 | 0.6745 | 3 |
| | E100A | 6.97 ± 0.18 | 0.6133 | 79.27 ± 6.72 | 0.1533 | 3 |
| | F105A | 6.77 ± 0.15 | 0.1851 | 57.39 ± 4.17**** | <0.0001 | 3 |
| | T121A | 6.14 ± 0.41*** | 0.0007 | 31.53 ± 7.09**** | <0.0001 | 3 |
| | R194A | 6.55 ± 0.19* | 0.0339 | 81.10 ± 7.60 | 0.2549 | 3 |
| | R208A | 6.58 ± 0.16* | 0.0431 | 52.09 ± 4.26**** | <0.0001 | 3 |
| | K273A | 5.73 ± 0.18**** | <0.0001 | 68.51 ± 8.34** | 0.0035 | 3 |
| | H299A | 8.44 ± 0.24* | 0.0164 | 36.04 ± 4.01**** | <0.0001 | 3 |
| | L118S+V122S | 6.14 ± 0.18*** | 0.0007 | 84.85 ± 8.36 | 0.5869 | 3 |
| | Q205H | 6.17 ± 0.46*** | 0.001 | 25.10 ± 6.36**** | <0.0001 | 3 |
| | R208K | 6.69 ± 0.22 | 0.1016 | 60.43 ± 6.52*** | 0.0001 | 3 |
| | T295V | 7.19 ± 0.33 | 0.9657 | 30.00 ± 4.54**** | <0.0001 | 4 |

Inhibition of forskolin-induced cAMP accumulation was performed in HEK293T cells transiently transfected with WT and mutant receptors. All the mutant constructs were modified by single-point mutation in the setting of the WT receptor. cAMP accumulation data were analyzed using a three-parameter logistic equation to determine $p\mathrm{EC}_{50}$ and $\mathrm{E}_{max}$ values. $\mathrm{E}_{max}$ values for mutants are defined as the window between the maximal response and vehicle control (no ligand) and expressed as a percentage of the WT. Cell surface expression was assessed by flow cytometry to detect the N-terminal Flag epitope label on the receptors and normalized to the WT receptor (shown as percentage). Data shown are means ± S.E.M. of at least three independent experiments. One-way ANOVA were used to determine statistical difference (*$P$< 0.05, **$P$< 0.01, ***$P$< 0.001 and ****$P$< 0.0001). $n$, sample size; the number of independent experiments. N.A., not active.

**Supplementary Table 5.** Effects of key residues mutation on receptor subtype selectivity.

| Receptor | Mutation | INSL5 | | | | | Relaxin-3 | | | | |
|---|---|---|---|---|---|---|---|---|---|---|---|
| | | $pEC_{50}$ | | $E_{max}$ (% WT) | | *n* | $pEC_{50}$ | | $E_{max}$ (% WT) | | *n* |
| | | Means ± S.E.M. | *P* value | Means ± S.E.M. | *P* value | | Means ± S.E.M. | *P* value | Means ± S.E.M. | *P* value | |
| RXFP4 | WT | 9.02 ± 0.09 | —— | 98.86 ± 3.65 | —— | 6 | 8.74 ± 0.10 | —— | 95.70 ± 4.30 | —— | 7 |
| | T295V | 9.16 ± 0.17 | 0.8687 | 91.17 ± 6.47 | 0.5243 | 3 | 9.23 ± 0.20 | 0.2688 | 77.70 ± 6.32 | 0.2278 | 3 |
| | L118S+V122S | N.A. | —— | N.A. | —— | 3 | 7.40 ± 0.14**** | <0.0001 | 106.69 ± 7.69 | 0.7224 | 3 |
| | L118A+V122A | N.A. | —— | N.A. | —— | 4 | 7.75 ± 0.18** | 0.0011 | 96.13 ± 8.52 | >0.9999 | 4 |
| | L118A | N.A. | —— | N.A. | —— | 3 | 8.01 ± 0.14* | 0.0361 | 99.73 ± 6.19 | 0.9975 | 3 |
| | L118S | N.A. | —— | N.A. | —— | 3 | 8.23 ± 0.17 | 0.2305 | 92.78 ± 6.88 | 0.9996 | 3 |
| | V122A | 8.44 ± 0.23 | 0.0728 | 33.20 ± 3.27**** | <0.0001 | 3 | 8.20 ± 0.31 | 0.1719 | 31.24 ± 4.24**** | <0.0001 | 3 |
| | V122S | 8.99 ± 0.26 | 0.9995 | 45.95 ± 4.97**** | <0.0001 | 3 | 7.69 ± 0.27** | 0.0016 | 49.66 ± 6.44*** | 0.0001 | 3 |
| RXFP3 | WT | N.D. | —— | N.D. | —— | —— | 8.99 ± 0.09 | —— | 101.40 ± 3.62 | —— | 3 |
| | V375T | N.D. | —— | N.D. | —— | —— | 8.28 ± 0.41 | 0.3706 | 66.57 ± 11.87* | 0.0169 | 3 |
| | S159L+S163V | N.D. | —— | N.D. | —— | —— | 8.41 ± 0.23 | 0.5638 | 72.69 ± 7.22 | 0.0562 | 3 |
| | S159A+S163A | N.D. | —— | N.D. | —— | —— | 8.96 ± 0.38 | 0.9999 | 43.57 ± 6.93*** | 0.0002 | 3 |
| | S159L | N.D | —— | N.D. | —— | —— | 8.13 ± 0.17 | 0.2088 | 81.00 ± 6.00 | 0.2470 | 3 |
| | S159A | N.D. | —— | N.D. | —— | —— | 8.41 ± 0.25 | 0.5624 | 65.67 ± 7.00* | 0.0141 | 3 |
| | S163V | N.D. | —— | N.D. | —— | —— | 8.87 ± 0.26 | 0.9996 | 36.91 ± 4.14**** | <0.0001 | 3 |
| | S163A | N.D. | —— | N.D. | —— | —— | 9.12 ± 0.34 | 0.9995 | 48.85 ± 6.78*** | 0.0005 | 3 |

Inhibition of forskolin-induced cAMP accumulation was performed in HEK293T cells transiently transfected with WT and mutant receptors. All the mutant constructs were modified by single-point mutation in the setting of the WT receptor. cAMP accumulation data were analyzed using a three-parameter logistic equation to determine $pEC_{50}$ and $E_{max}$ values. $E_{max}$ values for mutants are defined as the window between the maximal response and vehicle control (no ligand) and expressed as a percentage of the WT. Data shown are means ± S.E.M. of at least three independent experiments. One-way ANOVA were used to determine statistical difference (*$P$< 0.05, **$P$< 0.01, ***$P$< 0.001 and ****$P$< 0.0001). *n*, sample size; the number of independent experiments. N.A., not active; N.D., not determined.

**Supplementary Table 6 |** Primers used in this study, related to Figures 2 and 3, Supplementary Figures 3 and 10 and Supplementary Tables 3, 4 and 5.

| Oligonucleotide name | Oligonucleotide sequence (5'-3') | Cloning method | Product |
|---|---|---|---|
| Insert-fragment-forward | AGATCTGCGCCGCGATCGCCCAAAATGAAGAC GATCATCGCC | Homologous recombination | pCMV6-HA-H10-BRIL-RXFP4(1-374)-LgBiT |
| Insert-fragment-reverse | CTATGACCGCGGCCGGCCGTTTAGCTGTTGATG GTTACTCGGAA | | |
| Linear-pCMV6-forward | ACGGCCGGCCGCGGTCAT | | |
| Linear-pCMV6-reverse | GGCGATCGCGGCGCAGAT | | |
| Add-RXFP4-Flag-forward | CGATCGCCATGGACTACAAAGACGATGACGAC AAGCCCACACTCAATACT | Site-directed mutagenesis | pCMV6-Flag-RXFP4 |
| Add-RXFP4-Flag-reverse | GAGTGTGGGCTTGTCGTCATCGTCTTTGTAGTC CATGGCGATCGCGGCGC | | |
| Add-RXFP3-Flag-forward | CTTGCCATGGACTACAAAGACGATGACGACAA GCAGATGGCCGATGCAGCCAC | | pCMV6-Flag-RXFP3 |
| Add-RXFP3-Flag-reverse | CTTGTCGTCATCGTCTTTGTAGTCCATGGCAAG CTTGGCGGCAGATCTC | | |
| W97A-forward | GCACTCACTCTCCCCTTTGCGGCAGCCGAG | Site-directed mutagenesis | pCMV6-RXFP4(1-374)-W97A |
| W97A-reverse | CTCGGCTGCCGCAAAGGGGAGAGTGAGTGC | | |
| E100A-forward | TTTTGGGCAGCCGCGTCGGCACTGGAC | | pCMV6-RXFP4(1-374)-E100A |
| E100A-reverse | GTCCAGTGCCGACGCGGCTGCCCAAAA | | |
| D104A-forward | GAGTCGGCACTGGCCTTTCACTGGCCC | | pCMV6-RXFP4(1-374)-D104A |
| D104A-reverse | GGGCCAGTGAAAGGCCAGTGCCGACTC | | |
| F105A-forward | GAGTCGGCACTGGACGCTCACTGGCCCTTCGG | | pCMV6-RXFP4(1-374)-F105A |
| F105A-reverse | CCGAAGGGCCAGTGAGCGTCCAGTGCCGACTC | | |
| T121A-forward | TGGTTCTGACGGCCGCTGTCCTCAACGT | | pCMV6-RXFP4(1-374)-T121A |
| T121A-reverse | GACGTTGAGGACAGCGGCCGTCAGAACCA | | |
| R194A-forward | GCCTTTGCCTGCTGGCTTTCCCCAGCAGGT | | pCMV6-RXFP4(1-374)-R194A |
| R194A-reverse | ACCTGCTGGGGAAAGCCAGCAGGCAAAGGC | | |
| Q205A-forward | GCTGGGGGCCTACGCGCTGCAGAGGGTG | | pCMV6-RXFP4(1-374)-Q205A |
| Q205A-reverse | CACCCTCTGCAGCGCGTAGGCCCCCAGC | | |
| R208A-forward | CCTACCAGCTGCAGGCGGTGGTGCTGGCTT | | pCMV6-RXFP4(1-374)-R208A |
| R208A-reverse | AAGCCAGCACCACCGCCTGCAGCTGGTAGG | | |

| | | | |
|---|---|---|---|
| K273A-forward | TGGGGTGTCCTGGTGGCGTTTGACCTGGTGCC | | pCMV6-RXFP4(1-374)-K273A |
| K273A-reverse | GGCACCAGGTCAAACGCCACCAGGACACCCCA | | |
| W279A-forward | GAAGTTTGACCTGGTGCCCGCGAACAGTACTTTCTATACTA | | pCMV6-RXFP4(1-374)-W279A |
| W279A-reverse | TAGTATAGAAAGTACTGTTCGCGGGCACCAGGTCAAACTTC | | |
| Y284A-forward | GCCCTGGAACAGTACTTTCGCTACTATCCAGACGTATGTC | | pCMV6-RXFP4(1-374)-Y284A |
| Y284A-reverse | GACATACGTCTGGATAGTAGCGAAAGTACTGTTCCAGGGC | | |
| T295A-forward | TGTCTTCCCTGTCACTGCTTGCTTGGCACACAG | | pCMV6-RXFP4(1-374)-T295A |
| T295A-reverse | CTGTGTGCCAAGCAAGCAGTGACAGGGAAGACA | | |
| H299A-forward | GTCACTACTTGCTTGGCAGCCAGCAATAGCTGCCTCAA | | pCMV6-RXFP4(1-374)-H299A |
| H299A-reverse | TTGAGGCAGCTATTGCTGGCTGCCAAGCAAGTAGTGAC | | |
| Q205H-forward | GGGGGCCTACCATCTGCAGAGGGTG | | pCMV6-RXFP4(1-374)-Q205H |
| Q205H-reverse | CACCCTCTGCAGATGGTAGGCCCCC | | |
| R208K-forward | GGCCTACCAGCTGCAGAAGGTGGTGCT | | pCMV6-RXFP4(1-374)-R208K |
| R208K-reverse | AGCACCACCTTCTGCAGCTGGTAGGCC | | |
| T295V-forward | GCCCTCTGCAAGATGGTTTCGACGGCCACTAGCCTCAACGTCTATGC | | pCMV6-RXFP4(1-374)-T295V |
| T295V-reverse | GCATAGACGTTGAGGCTAGTGGCCGTCGAAACCATCTTGCAGAGGGC | | |
| L118S+V122S-forward | GCCCTCTGCAAGATGGTTTCGACGGCCACTAGCCTCAACGTCTATGC | | pCMV6-RXFP4(1-374)-L118S+V122S |
| L118S+V122S-reverse | GCATAGACGTTGAGGCTAGTGGCCGTCGAAACCATCTTGCAGAGGGC | | |
| L118A+V122A-forward | GTGCCCTCTGCAAGATGGTTGCGACGGCCACTG | | pCMV6-RXFP4(1-374)-L118A+V122A |
| L118A+V122A-reverse | CAGTGGCCGTCGCAACCATCTTGCAGAGGGCAC | | |
| L118A-forward | TTCTGACGGCCACTGCCCTCAACGTCTATGCCAGCA | | pCMV6-RXFP4(1-374)-L118A |
| L118A-reverse | ATAGACGTTGAGGGCAGTGGCCGTCAGAACCATCTT | | |
| V122A-forward | GTGCCCTCTGCAAGATGGTTTCGACGGCCACTG | | pCMV6-RXFP4(1-374)-L118S |
| V122A-reverse | CAGTGGCCGTCGAAACCATCTTGCAGAGGGCAC | | |

| | | | |
|---|---|---|---|
| L118S-forward | TCTGACGGCCACTAGCCTCAACGTCTATGCCAGCATC | | pCMV6-RXFP4(1-374)-V122A |
| L118S-reverse | GGCATAGACGTTGAGGCTAGTGGCCGTCAGAACCATCT | | |
| V122S-forward | AAGATGGTTGCGACGGCCACTGCCCTCAACGTC | | pCMV6-RXFP4(1-374)-V122S |
| V122S-reverse | TTGAGGGCAGTGGCCGTCGCAACCATCTTGCA | | |
| H268Q-forward | TGGCTGGGCCTCTACCAGTCGCAGAAG | Site-directed mutagenesis | pCMV6-RXFP3(1-469)-H268Q |
| H268Q-reverse | CTTCTGCGACTGGTAGAGGCCCAGCCA | | |
| K271R-forward | GGCCTCTACCACTCGCAGAGGGTGCTGCTG | | pCMV6-RXFP3(1-469)-K271R |
| K271R-reverse | CAGCAGCACCCTCTGCGAGTGGTAGAGGCC | | |
| V375T-forward | GCGTTCCCTGTGAGCACGTGCCTAGCGCACTC | | pCMV6-RXFP3(1-469)-V375T |
| V375T-reverse | GAGTGCGCTAGGCACGTGCTCACAGGGAACGC | | |
| S159L+S163V-forward | GCCATGTGTAAGATCGTGTTAATGGTGACGGTCATGAACATGTACGCCAGC | | pCMV6-RXFP3(1-469)-S159L + S163L |
| S159L+S163V-reverse | GCTGGCGTACATGTTCATGACCGTCACCATTAACACGATCTTACACATGGC | | |
| S159L+S163A-forward | TAAGATCGTGGCCATGGTGACGGCCATGAACATGTACGCC | | pCMV6-RXFP3(1-469)-S159A + S163A |
| S159A+S163A-reverse | ATGTTCATGGCCGTCACCATGGCCACGATCTTACACATGG | | |
| S159A-forward | CCATGTGTAAGATCGTGGCCATGGTGACGTCCATG | | pCMV6-RXFP3(1-469)-S159A |
| S159A-reverse | CATGGACGTCACCATGGCCACGATCTTACACATGG | | |
| S163A-forward | TCCATGGTGACGGCCATGAACATGTACGCCAGCGTGT | | pCMV6-RXFP3(1-469)-S163A |
| S163A-reverse | GCGTACATGTTCATGGCCGTCACCATGGACACGATCTT | | |
| S159L-forward | GCCATGTGTAAGATCGTGTTAATGGTGACGTCCATGAACA | | pCMV6-RXFP3(1-469)-S159L |
| S159L-reverse | TGTTCATGGACGTCACCATTAACACGATCTTACACATGGC | | |
| S163V-forward | ATCGTGTCCATGGTGACGGTCATGAACATGTACGCCAG | | pCMV6-RXFP3(1-469)-S163V |
| S163V-reverse | CTGGCGTACATGTTCATGACCGTCACCATGGACACGAT | | |

**Supplementary Table 7.** Details of restraints applied during MD simulations.

| Stage | Time step | Simulation time | Restrain |
|---|---|---|---|
| Heating | 1 fs | 1 ns | Position harmonic restrain (40 kJ·mol$^{-1}$·Å$^{-2}$) for the backbone non-hydrogen atoms of protein and peptide;<br>Position restrain (20 kJ·mol$^{-1}$·Å$^{-2}$) for the sidechain non-hydrogen atoms of protein and peptide;<br>Planar harmonic restraint (10 kJ·mol$^{-1}$·Å$^{-2}$) for the phosphorus atom of POPC along the Z-axis;<br>Dihedral restraint (1000 kJ·mol$^{-1}$·rad$^{-2}$) for two dihedrals (C28-C29-C210-C211 and C1-C3-C2-O21). |
| Step6.1 | 1 fs | 5 ns | Position harmonic restrain (40 kJ·mol$^{-1}$·Å$^{-2}$) for the backbone non-hydrogen atoms of protein and peptide;<br>Position restrain (20 kJ·mol$^{-1}$·Å$^{-2}$) for the sidechain non-hydrogen atoms of protein and peptide;<br>Planar harmonic restraint (10 kJ·mol$^{-1}$·Å$^{-2}$) for the phosphorus atom of POPC along the Z-axis;<br>Dihedral restraint (1000 kJ·mol$^{-1}$·rad$^{-2}$) for two dihedrals (C28-C29-C210-C211 and C1-C3-C2-O21). |
| Step6.2 | 1 fs | 5 ns | Position harmonic restrain (20 kJ·mol$^{-1}$·Å$^{-2}$) for the backbone non-hydrogen atoms of protein and peptide;<br>Position restrain (10 kJ·mol$^{-1}$·Å$^{-2}$) for the sidechain non-hydrogen atoms of protein and peptide;<br>Planar harmonic restraint (4 kJ·mol$^{-1}$·Å$^{-2}$) for the phosphorus atom of POPC along the Z-axis;<br>Dihedral restraint (400 kJ·mol$^{-1}$·rad$^{-2}$) for two dihedrals (C28-C29-C210-C211 and C1-C3-C2-O21). |
| Step6.3 | 2 fs | 10 ns | Position harmonic restrain (10 kJ·mol$^{-1}$·Å$^{-2}$) for the backbone non-hydrogen atoms of protein and peptide;<br>Position restrain (5 kJ·mol$^{-1}$·Å$^{-2}$) for the sidechain non-hydrogen atoms of protein and peptide;<br>Planar harmonic restraint (4 kJ·mol$^{-1}$·Å$^{-2}$) for the phosphorus atom of POPC along the Z-axis; |

| | | | |
|---|---|---|---|
| | | | Dihedral restraint (200 $kJ \cdot mol^{-1} \cdot rad^{-2}$) for two dihedrals (C28-C29-C210-C211 and C1-C3-C2-O21). |
| Step6.4 | 2 fs | 10 ns | Position harmonic restrain (5 $kJ \cdot mol^{-1} \cdot Å^{-2}$) for the backbone non-hydrogen atoms of protein and peptide;<br>Position restrain (2 $kJ \cdot mol^{-1} \cdot Å^{-2}$) for the sidechain non-hydrogen atoms of protein and peptide;<br>Planar harmonic restraint (2 $kJ \cdot mol^{-1} \cdot Å^{-2}$) for the phosphorus atom of POPC along the Z-axis;<br>Dihedral restraint (200 $kJ \cdot mol^{-1} \cdot rad^{-2}$) for two dihedrals (C28-C29-C210-C211 and C1-C3-C2-O21). |
| Step6.5 | 2 fs | 10 ns | Position harmonic restrain (2 $kJ \cdot mol^{-1} \cdot Å^{-2}$) for the backbone non-hydrogen atoms of protein and peptide;<br>Position restrain (0.5 $kJ \cdot mol^{-1} \cdot Å^{-2}$) for the sidechain non-hydrogen atoms of protein and peptide;<br>Planar harmonic restraint (0.4 $kJ \cdot mol^{-1} \cdot Å^{-2}$) for the phosphorus atom of POPC along the Z-axis;<br>Dihedral restraint (100 $kJ \cdot mol^{-1} \cdot rad^{-2}$) for two dihedrals (C28-C29-C210-C211 and C1-C3-C2-O21). |
| Step6.6 | 2 fs | 10 ns | Position harmonic restrain (0.5 $kJ \cdot mol^{-1} \cdot Å^{-2}$) for the backbone non-hydrogen atoms of protein and peptide; |
| Step7 | 2 fs | 1000 ns | Restrain-free |

**Supplementary References**


1 Cherezov, V. *et al.* High-resolution crystal structure of an engineered human $\beta_2$-adrenergic G protein-coupled receptor. *Science* **318**, 1258-1265 (2007).

2 Zhang, X. *et al.* Structures of the human cholecystokinin receptors bound to agonists and antagonists. *Nat Chem Biol* **17**, 1230-1237 (2021).

3 Yin, Y. L. *et al.* Molecular basis for kinin selectivity and activation of the human bradykinin receptors. *Nat Struct Mol Biol* **28**, 755-761 (2021).

4 Zhu J. *et al.* Identification of the domains in RXFP4 (GPCR142) responsible for the high affinity binding and agonistic activity of INSL5 at RXFP4 compared to RXFP3 (GPCR135). *Eur J Pharmacol* **590**, 43-52 (2008).